



Repositorio Institucional de la Universidad Autónoma de Madrid

<https://repositorio.uam.es>

Esta es la **versión de autor** del artículo publicado en:
This is an **author produced version** of a paper published in:

Inorganic Chemistry 58.5 (2019): 3290-3301

DOI: <https://doi.org/10.1021/acs.inorgchem.8b03364>

Copyright: © 2019 American Chemical Society

El acceso a la versión del editor puede requerir la suscripción del recurso
Access to the published version may require subscription

Multifunctional Cu(I) Coordination Polymers with Aromatic Mono- and Ditopic Thioamides

Javier Troyano,[†] Eduardo Zapata,[†] Josefina Perles,[§] Pilar Amo-Ochoa,^{&†} Vanesa Fernández-Moreira,[‡] José I. Martínez,^φ Félix Zamora,^{□,†,&} and Salomé Delgado,^{†,&*}*

[†]Departamento de Química Inorgánica, Universidad Autónoma de Madrid, 28049 Madrid, Spain;

[§]Servicio Interdepartamental de Investigación. Universidad Autónoma de Madrid, 28049 Madrid,

Spain; [‡]Departamento de Química Inorgánica, Instituto de Síntesis Química y Catálisis

Homogénea (ISQCH), CSIC-Universidad de Zaragoza, Zaragoza 50009, Spain; [&]Institute for

Advanced Research in Chemical Sciences (IAdChem) Universidad Autónoma de Madrid, 28049

Madrid, Spain; ^φDepartamento de Nanoestructuras, Superficies, Recubrimientos y Astrofísica

Molecular, Instituto de Ciencia de Materiales de Madrid (ICMM-CSIC), 28049 Madrid, Spain;

[□]Instituto Madrileño de Estudios Avanzados en Nanociencia (IMDEA Nanociencia),

Cantoblanco, 28049 Madrid, Spain.

Keywords: Coordination Polymers, Luminescence, Fluorescence, Thioamides.

Abstract

Direct reactions under ambient conditions between CuX (X= Br, I) and thiobenzamide (TBA) were carried out at different ratios giving rise to the formation of a series of one-dimensional

coordination polymers (1D-CPs) $[\text{CuI}(\text{TBA})]_n$ (**1**), $[\text{CuI}(\text{TBA})]_n$ (**4**) and $[\text{CuBr}(\text{TBA})]_n$ (**5**), as well as two molecular complexes $[\text{CuI}(\text{TBA})_3]$ (**2**) and $[\text{Cu}_2\text{I}_2(\text{TBA})_4] \cdot 2\text{MeCN}$ (**3**).

Recrystallization of **1** and **5** yielded a series of isostructural 1D-CPs solvated species $[\text{CuI}(\text{TBA}) \cdot \text{S}]_n$ (**1**·S) (S= THF, acetone, methanol) and $[\text{CuBr}(\text{TBA}) \cdot \text{S}]_n$ (**5**·S) (S=THF, acetone), respectively. Similar reactions between CuI and dithiobenzamide (DTBA) allowed to isolate a series of 2D-CPs $[\text{CuI}(\text{DTBA}) \cdot \text{S}]_n$ (S= DMF, acetonitrile and methanol) (**6**·S). Interestingly, **1**·S and **5**·S showed variable luminescence and electrical semiconductivity depending on the different solvents located in their structures. Thus, **1** and **5** could display potential application for sensing volatile organic vapors (VOCs) by virtue of the significant changes in their emission upon solvent exposure, even by naked eye. Theoretical calculations have been used to rationalize these electronic properties.

Introduction

Coordination polymers (CPs) have attracted increasing attention in recent years due to their interesting architectures and physico-chemical properties.¹ In particular, those with Cu(I) are relevant because of their structural diversity, electrical conductivity² and luminescence properties.³ Additionally, the development of new systems based on Cu(I) is strongly motivated by its low toxicity, low cost and availability of copper compared to the noble metals and rare earths.⁴ Among these systems, Cu(I) halides represent a versatile type of building blocks that have been successfully used for the synthesis of CPs in combination with different neutral ligands and offer appreciable optoelectronic properties.⁵ On the other hand, organosulfur-containing ligands have

demonstrated their potential as linkers in the synthesis of metal–organic networks showing interesting electrical and luminescence properties.⁶

Although heterocyclic thioamides constitute an important class of sulfur-containing organic compounds that have been largely studied for their interesting chemical, biochemical, structural and spectroscopic properties,⁷ structurally simple thioamides, such as thiobenzamide (TBA) and dithiobenzamide (DTBA), have been scarcely developed in the field of supramolecular chemistry.⁸ Indeed, thioamides are very versatile ligands in their coordination modes due to the presence of nitrogen and sulfur donor sites. They have the ability to behave as bidentate chelate or bridging ligands or as monodentate “soft” ligands *via* S-coordination or “hard” ligands through N-site. Thus, in complexes of TBA or DTBA with “soft” ions as copper(I) those ligands compete with “soft” anions such as the heavier halide ions. Additionally, the hydrogen bond interactions of amide groups could play an essential role in the auto assembly process.

As we have previously established that CPs based on Cu(I) with organosulfur ligands are highly desirable to obtain materials with multifunctional properties,^{2c, 2d, 9} in this work we have focused on the potential of the TBA and DTBA to produce multifunctional materials with electrical conductivity and photoluminescence.

Experimental Section

Materials and Methods. All the reagents were purchased from Sigma-Aldrich and used as received. The ligand 1,4-dithiobenzamide (DTBA) was prepared by a previously published method.¹⁰ FTIR spectra (KBr pellets) were recorded using a Perkin-Elmer 1650 spectrophotometer. C, H, N, S elemental analyses were performed by using a Perkin-Elmer 240

B microanalyser. X-ray powder diffraction (XRPD) experiments were carried out using a PANalytical X'Pert PRO diffractometer with a theta/2theta primary monochromator and a fast X'Celerator detector. The samples were analyzed with scanning theta/2theta. Steady state photoluminescence spectra were recorded on a Jobin-Yvon Horiba Fluorolog FL-3-11 spectrometer using band pathways of 3 nm for both excitation and emission. Phosphorescence lifetimes were recorded with an IBH 5000F coaxial nanosecond flashlamp. The lifetime data were fitted with the Jobin-Yvon software package. Measurements at variable temperature were done with an Oxford Cryostat Optistat DN. The lifetime data were fitted using the Jobin-Yvon IBH software DAS6 v6.1.

X-ray Data Collection and Crystal Structure Determination. Data collection was carried out on a Bruker Kappa Apex II diffractometer, using graphite-monochromated Mo-K α radiation ($\lambda=0.71073$ Å) and operating at 50 kV and 30 mA. The crystal structures of compounds were determined by single-crystal X-ray diffraction at room temperature, except for the samples with low stability in normal conditions; in particular, the higher temperature data for **5** was collected at 250 K and for **5**·acetone and **6** MeCN only a low temperature data collection was made (at 200 and 100 K respectively). Additionally, compounds **1**, **1**·S (S= THF, acetone, MeOH), **5**, **5**·THF and **6**·DMF were measured at 110 K to observe the influence of low temperature in the solid-state arrangement. Detailed information about the structural determination is collected in the Supporting Information (Figures S1-23 and Tables S1-67). Files in CIF format for the compounds are (CCDC refs.: 1835539-1835559) available free of charge.

In the structure of compound **6**·DMF, the atoms in the solvent molecules are not involved in hydrogen bonds in two different positions and a disorder model was done accordingly (Figure S13).

Direct Current (DC) Electrical Conductivity Determination. Electrical conductivity measurements were performed on different single crystals of **1**·acetone, **1**·MeOH, **4**, **5**·THF, **5**·acetone, **6**·DMF and in different compact pellets in case of **1**, **1**·THF and **5**. In all cases, except for compound **6**·DMF, the two contacts are made with carbon paint at 300 K. The small size of CP **6** crystals only allow direct two contacts with the metal tips (without the carbon paste). The contacts were made with platinum wires (25 μm diameter). The samples were measured at 300 K by applying an electrical current with voltages from +10 to -10 V.

Computational Methods. To analyze the electronic, optical and excitation properties of the different compounds in the present study we have performed a large battery of first-principles static, time-dependent DFT-based, and single-excitation calculations. A time-dependent DFT (TDDFT) formalism has been employed to compute the excitation spectra¹¹ as implemented in the plane-wave simulation package QUANTUM ESPRESSO distribution (<http://www.quantum-espresso.org>). In the calculations we have used the simulation cells and structures resolved at different temperatures as obtained by X-ray diffraction experiments, yielding residual forces acting on each atom below $0.1 \text{ eV}\text{\AA}^{-1}$, enough to guarantee fully converged results. In all the calculations Brillouin zones (BZs) were sampled by means of optimal Monkhorst–Pack grids.¹² Generalized gradient Perdew–Burke–Ernzerhof (PBE) functional has been used to account for the exchange–correlation (XC) effects,¹³ ultra-soft pseudopotentials to model the ion–electron interaction within each atom,¹⁴ and a plane-wave basis set up to a kinetic energy cut-off of 40 Ry and 300 Ry for the charge density. The excitation spectra are obtained as $I(\omega) \propto \omega \text{Im}[\bar{\alpha}(\omega)]$, where $\bar{\alpha}$ is the spherical average (average of the diagonal elements) of the dipole polarizability; an imaginary part of 0.002 Ry has been added to the frequency in order to smooth the emerging divergences of the polarizability. Additionally, once the different TDDFT spectra were obtained, we have carried out

a battery of calculations with the GAUSSIAN09 package¹⁵ to obtain oscillator strengths, and elucidate transitions and electronic states involved in the most intense excitations by using the same GGA-PBE functional and the rather large 6-311G* basis set. To compute the individual transitions we have used the configuration interaction single-excitation (CIS) formalism.¹⁶ This implementation is computationally very demanding, but provides excellent results in both closed-shell and open-shell systems.

Synthesis of the compounds

Synthesis of [CuI(TBA)]_n (1). CuI (0.190 g, 1.00 mmol) and TBA (0.137 g, 1.00 mmol) in acetonitrile (10 mL) were mixed and stirred until homogeneous solution was formed. Then the solvent was removed under vacuum until a red goeey oil was obtained. This oil was sonicated in hexane resulting in an orange solid after extracting solvent. This product was washed with diethyl ether and dried under vacuum (0.135 g, 41 % yield). Single crystals suitable for X-ray diffraction studies were obtained by heating an equimolar mixture of CuI and TBA at 135 °C for 10 min. Then, the obtained red solid was left to stand in *n*-BuOH overnight, affording orange prismatic crystals of **1**. Elemental analysis calcd. (%) for C₇H₇ICuNS: C, 25.66; H, 2.14; N, 4.28; S, 9.79. Found (%): C, 24.87; H, 2.14; N, 4.16; S, 9.50. FT-IR selected data (KBr, cm⁻¹): 3378(m), 3225 (m), 3149 (m), 2922 (m), 2854 (m), 1582 (vs), 1441 (m), 1397 (s), 1278 (s), 1168 (s), 1015 (w), 925 (w), 859 (s), 762 (s), 677 (vs).

Synthesis of {[CuI(TBA)]·THF}_n (1·THF) and [CuI(TBA)]·acetone_n (1·acetone). Single crystals suitable for X-ray diffraction studies were obtained by slow diffusion at room temperature of *n*-pentane into THF or acetone solutions of **1**. **1**·THF: Elemental analysis calcd. (%) for C₁₁H₁₅ICuNSO: C, 33.05; H, 3.75; N, 3.50; S, 8.02. Found (%): C, 32.29; H, 3.63; N, 3.46; S, 8.12. FT-IR selected data (KBr, cm⁻¹): 3242 (m), 3086 (m), 2975 (m), 2871 (m), 1651(s), 1464

(s), 1322 (m), 1303 (s), 1275 (vs), 1183 (m), 1051 (vs), 868 (s), 774 (s), 686 (vs). **1**·acetone: Elemental analysis calcd. (%) for C₁₀H₁₃ICuNSO: C, 31,14; H, 3,40; N, 3,63; S, 8,31. Found (%): C,34,70; H, 3,70; N, 4,15; S, 9, 69. FT-IR selected data (KBr, cm⁻¹): 3278 (m), 3148 (s), 1697 (vs), 1642 (vs), 1595 (m), 1463 (m), 1412 (m), 1363 (m), 1310 (m), 1271 (vs),1225 (vs), 1186 (m), 1088 (m), 870 (vs), 774 (vs), 694 (vs).

Synthesis of {[CuI(TBA)]·MeOH}_n (1·MeOH). To a solution of CuI (0.190 g, 1.00 mmol) and TBA (0.137 g, 1.00 mmol) in 1 mL acetonitrile, 20 mL of methanol were added. This mixture was allowed to stand in a Petri dish at room temperature. After evaporation of solvent, orange prismatic crystals, suitable for X-ray diffraction studies, were synthesized. The crystalline product was washed with methanol and dried at air (0.334 g, 93 % yield). Elemental analysis calcd. (%) for C₈H₁₁ICuNSO: C, 26,71; H, 3,08; N, 3,89; S, 8,91. Found (%): C, 25,83; H, 2,88; N, 3,72; S, 8,90. FT-IR selected data (KBr, cm⁻¹): 3503 (m), 3253 (m), 3028 (m), 1645 (s), 1449 (s), 1309 (s), 1268 (s), 1141 (m), 1081 (w), 996 (s), 876 (s), 755 (s), 671 (vs).

Synthesis of [CuI(TBA)₃] (2). Following the same procedure as previously described for **1** but using CuI:TBA (1:5 ratio) [CuI (0.038 g, 0.20 mmol) and TBA (0.137 g, 1.00 mmol)] instead, a yellow solid was isolated after vacuum extraction of solvent, washed with dichloromethane and dried under vacuum (0.061 g, 50 % yield). Single crystals suitable for X-ray diffraction studies were obtained by *n*-pentane vapor diffusion into a diethyl ether solution of **2**. Elemental analysis calcd. (%) for C₂₁H₂₁ICuN₃S₃: C, 41, 91; H, 3,52; N, 6,98; S, 15,94. Found (%): C, 42.32; H, 3.59; N, 7.17; S, 15.84. FT-IR selected data (KBr, cm⁻¹): 3344 (m), 3244 (m), 3156 (s), 1606 (vs), 1450 (m), 1318 (m), 1268 (m), 1180 (m), 874 (vs), 770 (vs), 704 (s), 691 (s).

Synthesis of [Cu₂I₂(TBA)₄]·MeCN (3). An equimolar mixture of CuI (0.762 g, 4.00 mmol) and TBA (0.549 g, 4.00 mmol) in acetonitrile (2 mL) was sonicated until homogeneous solution was

obtained. Then the solution was left to stand overnight whereupon **3** precipitated as orange prismatic crystals, suitable for X-ray diffraction analysis. The crystalline product was filtered off, washed with a water:MeCN (1:1) solvent mixture, water and dried at air (0.146 g, 14 % yield). Elemental analysis calcd. (%) for $C_{30}H_{31}I_2Cu_2N_5S_4$: C, 37,12; H, 3,22; N, 7,21; S, 13,21. Found (%): C, 36,53; H, 3,16; N, 7,18; S, 13,03. FT-IR selected data (KBr, cm^{-1}): 3334 (m), 3247 (m), 3157 (m), 2252 (w), 1611 (vs), 1442 (m), 1418 (m), 1311 (m), 1265 (s), 1211 (s), 1170 (m), 1028 (w), 926 (w), 877 (s), 768 (m), 687 (vs).

*Synthesis of $[Cu_3I_3(TBA)_2]_n$ (**4**).* It was prepared following a slight modification of the way used for **1**·MeOH. Thus, to a solution of CuI (0.190 g, 1.00 mmol) and TBA (0.137 g, 1.00 mmol) in acetonitrile (1 mL), 20 mL of methanol were added. Then, the mixture was stirred for 1 h, and the resulting yellow solid was washed with methanol and diethyl ether and dried under vacuum (0.134 g, 48 % yield). Single crystals for X-ray diffraction analysis were obtained by n-pentane vapor diffusion into an equimolar solution of CuI and TBA in MeOH:MeCN 2:1. Elemental analysis calcd. (%) for $C_{14}H_{14}I_3Cu_3N_2S_2$: C, 19.88; H, 1.67; N, 3.31; S, 7.58. Found (%): C, 19.93; H, 1.84; N, 3.28; S, 7.56. FT-IR selected data (KBr, cm^{-1}): 3346 (m), 3245 (m), 3159 (m), 1601 (vs), 1441 (m), 1420 (m), 1316 (s), 1258 (s), 1211 (s), 1150 (s), 1027 (w), 925 (w), 866 (s), 763 (s), 685 (vs).

*Synthesis of $[CuBr(TBA)]_n$ (**5**).* An equimolar solution of CuBr (0.143 g, 1.0 mmol) and TBA (0.137 g, 1.00 mmol) in acetonitrile (20 mL) was stirred at room temperature for 30 min. After solvent removal in vacuum, obtained orange solid was washed with diethyl ether and dried under vacuum (0,171 g, 61 % yield). Orange prismatic single crystals, suitable for X-ray diffraction studies, were obtained by slow evaporation of a **5** solution in acetonitrile at room temperature. Elemental analysis calcd. (%) for $C_7H_7BrCuNS$: C, 29.97; H, 2.51; N, 4.99; S, 11.40. Found (%):

C, 30.34; H, 2.62; N, 5.16; S, 11.18. FT-IR selected data (KBr, cm^{-1}): 3267 (m), 3082 (m), 1628 (s), 1456 (s), 1306 (m), 1258 (s), 1184 (m), 1128 (w), 1073 (w), 926 (w), 850 (s), 765 (s), 679 (vs).

*Synthesis of $\{[\text{CuBr}(\text{TBA})]\cdot\text{THF}\}_n$ (**5** $\cdot\text{THF}$) and $[\text{CuBr}(\text{TBA})]\cdot\text{acetone}\}_n$ (**5** $\cdot\text{acetone}$).* By a similar procedure to that previously described for **1** $\cdot\text{THF}$ and **1** $\cdot\text{acetone}$, by slow *n*-pentane diffusion into THF or acetone solutions of **5**, suitable crystals for X-ray diffraction of **5** $\cdot\text{THF}$ and **5** $\cdot\text{acetone}$ were obtained. **5** $\cdot\text{THF}$: Elemental analysis calcd. (%) for $\text{C}_{11}\text{H}_{15}\text{BrCuNSO}$: C, 37.46; H, 4.29; N, 3.97; S, 9.07. Found (%): C, 37.40; H, 4.24; N, 3.89; S, 8.96. FT-IR selected data (KBr, cm^{-1}): 3254 (m), 3090 (m), 2952 (m), 2865 (m), 1652 (s), 1595 (m), 1459 (s), 1304 (vs), 1276 (vs), 1183 (m), 1048 (vs), 865 (s), 775 (s), 688 (vs). **5** $\cdot\text{acetone}$: Elemental analysis calcd. (%) for $\text{C}_{10}\text{H}_{13}\text{BrCuNOS}$: C, 35.46; H, 3.87; N, 4.14; S, 9.47. Found (%): C, 34.71; H, 3.70; N, 4.14; S, 9.69. FT-IR selected data (KBr, cm^{-1}): 3233 (m), 3073 (m), 1696 (vs), 1658 (m), 1456 (m), 1420 (m), 1364 (m), 1324 (m), 1305 (s), 1280 (s), 1231 (s), 883 (m), 767 (vs), 691 (vs).

*Synthesis of $\{[\text{CuI}(\text{DTBA})]\cdot\text{DMF}\}_n$ (**6** $\cdot\text{DMF}$).* A solution of DTBA (0.098 g, 0.50 mmol) in DMF (1 mL) was added to a solution of CuI (0.095 g, 0.50 mmol) in acetonitrile (20 mL) and the mixture was stirred at room temperature for 1 h. The orange solid obtained was washed with MeCN:DMF (10:1) and diethyl ether and dried under vacuum. (0.210 g, 91 % yield). Single crystals suitable for X-ray diffraction studies were obtained by diffusion of an acetonitrile solution of CuI, into a solution of DTBA in DMF at room temperature. Elemental analysis calcd. (%) for $\text{C}_{11}\text{H}_{15}\text{ICuON}_3\text{S}_2$: C, 28.73; H, 3.29; N, 9.14; S, 13.95. Found (%): C, 28.78; H, 3.32; N, 9.29; S, 13.85. FT-IR selected data (KBr, cm^{-1}): 3421 (s), 3259 (s), 3157 (m), 2916 (m), 1610 (s), 1435 (m), 1319 (m), 1265 (m), 1014 (w), 877 (w), 847 (w).

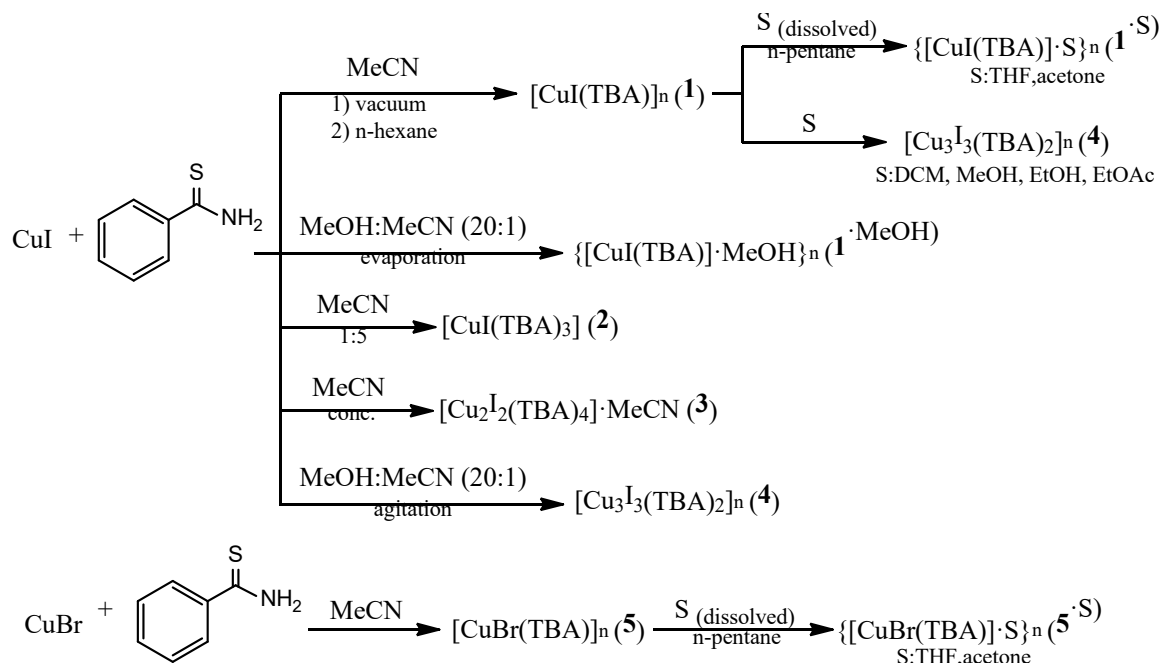
*Synthesis of $\{[\text{CuI}(\text{DTBA})]\cdot 2\text{MeCN}\}_n$ (**6** $\cdot 2\text{MeCN}$) and $\{[\text{CuI}(\text{DTBA})]\cdot\text{MeCN}\}_n$ (**6** $\cdot\text{MeCN}$).* A mixture of DTBA (0.019 g, 0.10 mmol) and CuI (0.019 g, 0.10 mmol) in acetonitrile (250 mL)

was refluxing for 30 min. An orange solution was obtained, which was filtered off and left to room temperature, giving rise to the obtention of orange crystals of **6**·2MeCN suitable for structure determination by X-ray diffraction. When these crystals were separated by filtration, washed with acetonitrile and diethyl ether and dried under vacuum, **6**·MeCN was obtained. (0.028 g, 65% yield). **6**·MeCN: Elemental analysis calcd. (%) for C₁₀H₁₁ICuN₃S₂: C, 28.08; H, 2.59; N, 9.82; S, 14.99. Found (%): C, 28.17; H, 2.67; N, 9.63; S, 14.90. FT-IR selected data (KBr, cm⁻¹): 3344 (m), 3253 (m), 3172 (m), 2281 (w), 2250 (w), 1628 (m), 1608 (s), 1434 (s), 1315 (m), 1263 (m), 1012 (w), 877 (m), 845 (m), 642 (m).

The phase purity of the as-synthesized compounds was confirmed by XRPD (Figures S24-34).

Results and Discussion

Synthesis and Structure of TBA based compounds. The synthetic route to this new class of CuX-TBA (X= I, Br) based compounds is gathered in Scheme 1. By mixing equimolar amounts of CuI and thiobenzamide (TBA) ligand in acetonitrile at room temperature, no precipitation from solution was observed, but after solvent removal, a red oil was obtained, leading after treatment with n-hexane, to polycrystalline [CuI(TBA)]_n (**1**). Interestingly, despite its polymeric structure **1** could be dissolved in THF and acetone, affording the corresponding solvated 1D CPs {[CuI(TBA)]·THF}_n (**1**·THF) and {[CuI(TBA)]·acetone}_n (**1**·acetone), respectively, after vapor diffusion of n-pentane. Analogous compound {[CuI(TBA)]·MeOH}_n (**1**·MeOH) was synthesized by direct reaction between CuI and TBA in MeOH:MeCN (10:1) solvent mixture.



Scheme 1. Synthetic routes of CuX-TBA (X= I, Br) coordination compounds formation.

The compounds **1** and **1**·S (S= THF, acetone, MeOH) display 1D polymeric chains, as depicted in Figure 1, parallel to the shortest cell axis (*b* in **1** and *a* in the solvated crystals). In all of the cases, the asymmetric unit contains one ligand, one iodine atom and one Cu(I) atom, plus one solvent molecule in the case of the structures **1**·THF, **1**·acetone and **1**·MeOH (Figures S1-S4).

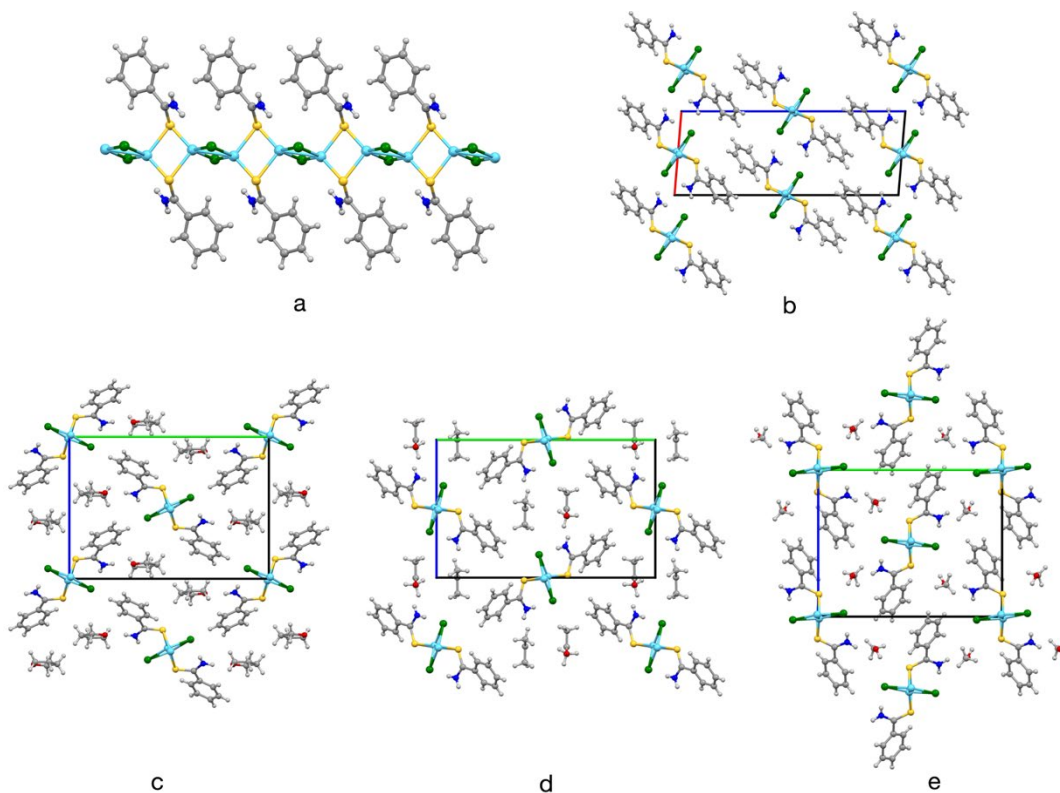


Figure 1. Lateral view of the 1D coordination polymer of **1** (a) and packing of the chains in the structures of **1** (b), **1**·THF (c) **1**·acetone, (d) and **1**·MeOH (e). (Cu: cyan, I: green, S: yellow, N: dark blue, O: red, C: gray, H: white).

Within the 1D chains, the copper atom is coordinated to two TBA ligands *via* the sulfur atom and to two iodine atoms in a Cu₂I₂S₂ environment. Additionally, Cu-Cu interactions can also be present, and the Cu-Cu distances are influenced by the presence of interstitial solvent molecules (Table S39-46). The polymeric chains contain alternated Cu₂I₂ and Cu₂S₂ rhombi at nearly perpendicular angles (80.98, 83.36, 82.33 and 81.73° for **1**, **1**·THF, **1**·acetone and **1**·MeOH, respectively).

Regarding the supramolecular arrangements, in compound **1** there are weak interchain N-H···I interactions, while stronger intrachain N-H···I hydrogen interactions are present (Table S63). In

the solvated cocrystals, there are also intrachain H-bonds; additionally, the interstitial solvent molecules in these structures are joined to the chains by N-H \cdots O hydrogen bonds in all of the cases (Table S63 and Figure S15). There are also weaker supramolecular O-H \cdots S and O-H \cdots I bonds in **1**·MeOH (Table S63).

The crystals of **1** and **1**·S adopt a needle or ribbon-like habit, and it was determined by the indexation of the crystal faces that the CP chains in these crystals are, in all the cases, oriented parallel to length of the crystals (Figures S20-21).

We also analyzed the influence of the stoichiometric ratio and the concentration of the reagents in the process of preparation. Thus, solutions with 2:1 and 1:2 CuI:TBA ratios in acetonitrile were treated in the same manner, but **1** was obtained in all the cases. Only when a large excess of TBA was used (5 eqv.), the molecular compound [CuI(TBA)₃] (**2**) was isolated showing a [CuI(TBA)₃] molecule per asymmetric unit (Figure 2a and S5). The copper(I) atom in this compound shows a tetrahedral CuIS₃ environment where the TBA ligands are coordinated by the S atom. There are N-H \cdots I interactions (both intra- and intermolecular) and N-H \cdots S hydrogen bonds between the [CuI(TBA)₃] molecules. Compound **2** was found to be isostructural with the previously reported chlorine derivative [CuCl(TBA)₃].¹⁷

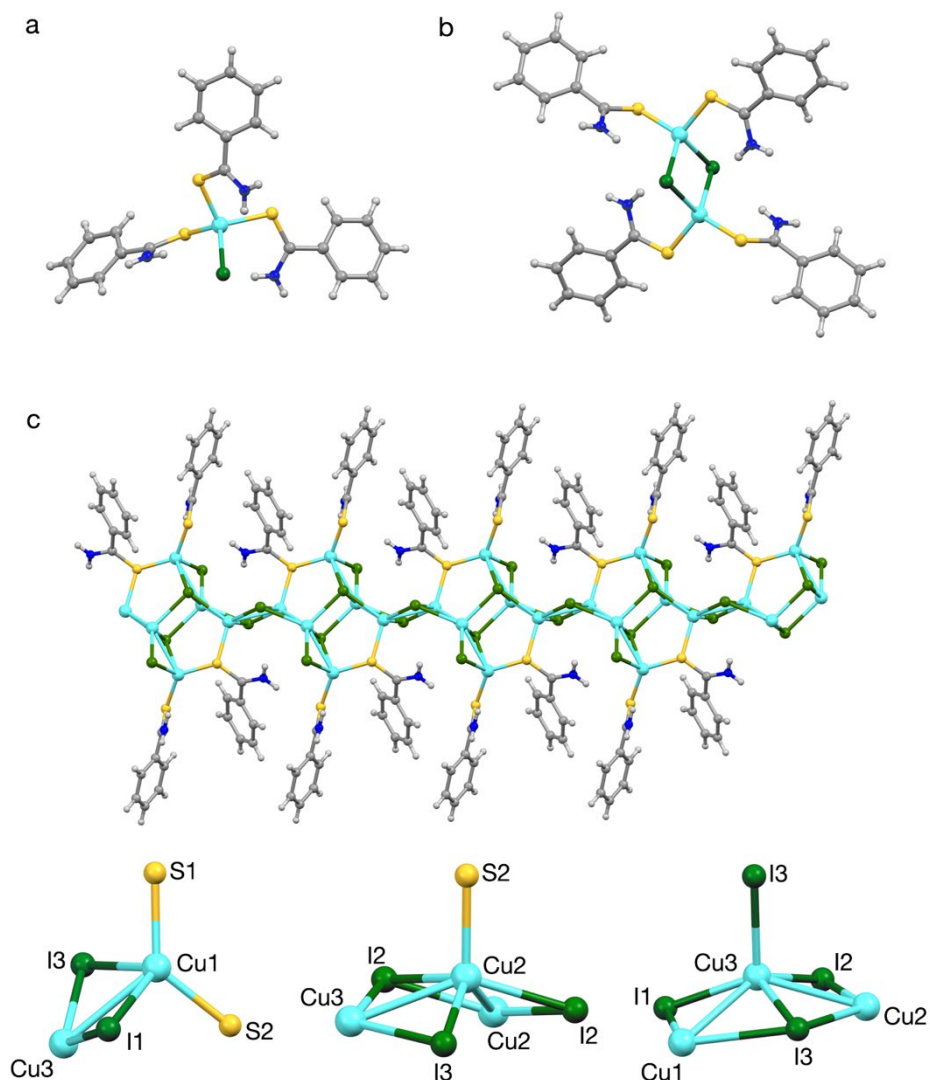


Figure 2. Molecular coordination compounds **2** (a) and **3** (b). Solvent molecules in **3** have been omitted. c) Polymeric $[\text{Cu}_3\text{I}_3(\text{TBA})_2]_n$ chain found in **4** (up) and copper environments for the three crystallographically independent copper atoms (bottom). (Cu: cyan, I: green, S: yellow, N: dark blue, O: red, C: gray, H: white).

In addition, when equimolar acetonitrile solutions of CuI and TBA at high concentrations (≥ 1 M) were left to stand undisturbed, the dimeric molecular complex $[\text{Cu}_2\text{I}_2(\text{TBA})_4] \cdot 2\text{MeCN}$ (**3**),

Figure 2b was obtained as a crystalline product. The asymmetric unit of **3** contains one copper(I) and one iodine atom, two TBA ligands and one MeCN interstitial molecule (Figure S6). This complex could be described as a molecular precursor of the $[\text{CuI}(\text{TBA})]_n$ CP chains, also showing the CuS_2I_2 coordination environment and the Cu_2I_2 rhombus observed in **1** and **1**·S. The packing of the dimers in the crystal could be described as chains of dimers joined by N-H \cdots S bonds along the *b* axis, with the solvent molecules bonded to the dimers by hydrogen N-H \cdots N bonds (Figure S16), analogous to the N-H \cdots O bonds observed in the solvated cocrystals of **1**. This dimeric molecule is similar to the previously reported $[\text{Cu}_2\text{I}_2(\text{TAA})_4]$.^{9b} Interestingly, the Cu-Cu distance in $[\text{Cu}_2\text{I}_2(\text{TBA})_4]$ was found to be considerably shorter (3.379 Å at 296 K) than the one in $[\text{Cu}_2\text{I}_2(\text{TAA})_4]$, 3.678 Å for the structure solved with the dataset collected at the same temperature. This distance gets shortened, as expected, in the structure of $[\text{Cu}_2\text{I}_2(\text{TBA})_4]$ solved from the data collected at low temperature (3.320 Å).

During our investigations, transformation of **1** into one-dimensional CP $[\text{Cu}_3\text{I}_3(\text{TBA})_2]_n$ (**4**) was observed after immersion of **1** in several solvents (Figure S34). The direct synthesis of **4** was carried out by stirring a equimolar solution of CuI and TBA in a MeOH:MeCN (20:1) solvent mixture, as shown in Scheme 1. Compound **4** displays a 1D structure which is different to that observed in compound **1**, as well as a different stoichiometry. The asymmetric unit contains three copper(I) centers, three iodine atoms and two TBA ligands (Figure S7). One of the TBA ligands shows the same coordination mode observed in compound **1** (S-donor monotopic), but the other ligand is acting μ_2 -S between copper atoms Cu1 and Cu2. (Figure 2c). Regarding the iodine atoms, μ_2 -I1 binds the metal centers Cu1 and Cu3, while μ_3 -I2 connects three copper atoms (Cu2, Cu2 and Cu3) and μ_4 -I3 is joining four metal centers (Cu1, Cu2 and Cu3). The three copper atoms in the asymmetric unit display also different environments, involving metal-metal interactions added

to the tetrahedral environment (Figure 2c, bottom). Unfortunately, these metal-metal interactions do not propagate along the full length of the CP, yielding only 6-member chains (Cu1-Cu3-Cu2-Cu2-Cu3-Cu1) as depicted in Figure S8.

The chains are packed in the crystal by van der Waals forces, while intrachain strong N-H \cdots S and weaker N-H \cdots I interactions can be observed. The orientation of the chains in the needle-shaped crystals was studied with the indexing of the faces in the measured crystals, and it was observed that the polymeric chains were oriented parallel to the longest axis of the single crystals (Figure S22).

For comparison, we also carried out the direct reaction between CuBr and TBA in acetonitrile at room temperature, giving rise to the formation of [CuBr(TBA)]_n (**5**). This 1D polymeric compound displays the same formula as the iodine derivative **1**, although there are important structural differences between the two CPs (Figure 3a). The asymmetric unit in **5** (Figure S9) is twice the one found in **1** (containing two copper atoms, two TBA ligands and two bromine atoms). More significantly, in the chains observed in compound **1** as well as in the solvated cocrystals, there are alternated Cu₂I₂ and Cu₂S₂ rhombi, while in the chains present in **5** there is only a Cu₂IS rhombus (with an angle between consecutive rhombi of 83.86). This leads to very similar Cu-Cu distances in **5**, while in **1** and the solvated compounds there are alternated shorter and longer ones. It is also remarkable the different supramolecular arrangement of the chains in **5** compared to that observed in **1**. In the bromine derivative, N-H \cdots Br interactions involving atoms within the same chain and from neighbor ones are very similar, while in compound **1** the interactions between atoms from adjacent 1D polymers were considerably weaker.

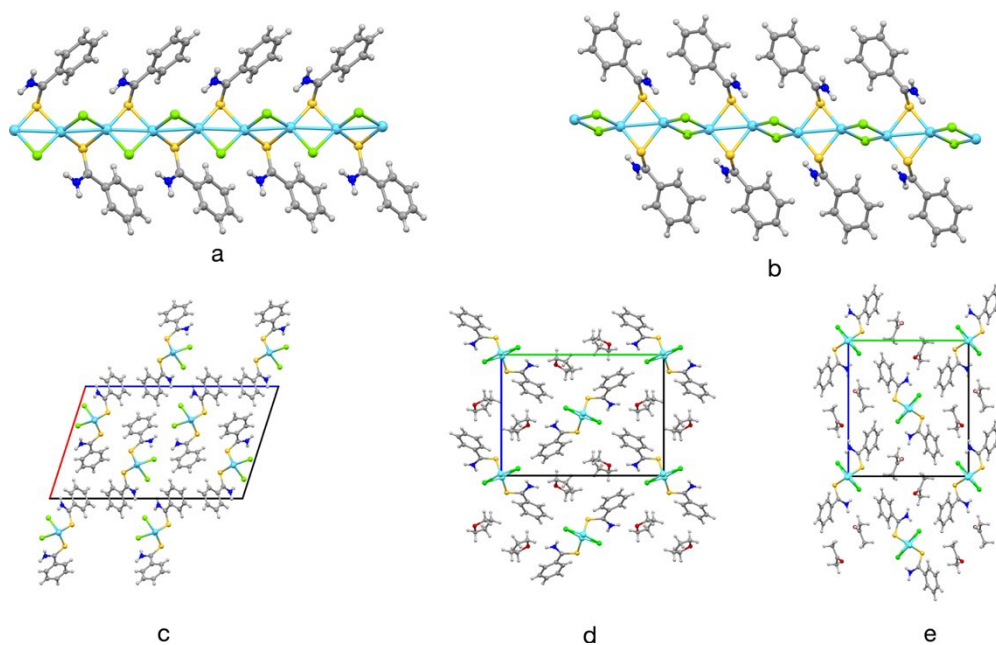


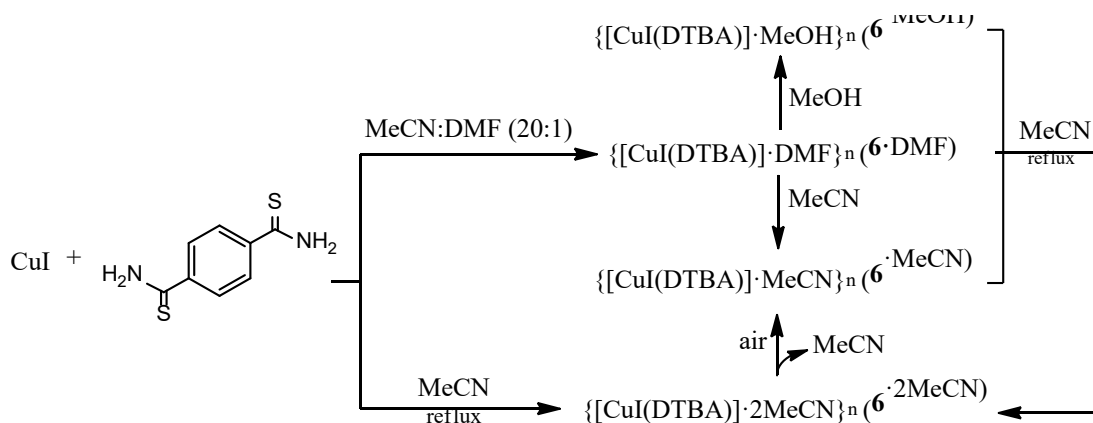
Figure 3. Lateral view of the 1D coordination polymer of **5** (a) and **5·S** (b) where S = THF or acetone; packing of the chains in the structures of **5** (c); **5·THF** (d) and **5·acetone** (e) (Cu: cyan, I: green, S: yellow, N: dark blue, O: red, C: gray, H: white).

Similarly to **1**, solubilization of **5** in THF and acetone allowed us to synthesize the corresponding $\{[\text{CuBr}(\text{TBA})] \cdot \text{THF}\}_n$ (**5·THF**) and $\{[\text{CuBr}(\text{TBA})] \cdot \text{acetone}\}_n$ (**5·acetone**), respectively. These compounds show a 1D CP analogous to the iodine derivatives, with the same alternating Cu_2I_2 and Cu_2S_2 rhombi pattern (Figure 3b, 3d and 3e). The asymmetric unit in both cocrystals of **5** is analogous to the corresponding solvated compounds of **1** as shown in Figures S10 and S11, and their supramolecular arrangement is also very similar (Figures 3 and S17); in particular **1·THF** and **5·THF**, they were found to be fully isostructural. In the case of **5** no transformations were noticed, as shown in Figure S36.

The crystals of compound **5** also adopt a needle or ribbon-like habit, and it was determined by the indexation of the crystal faces that the CP chains in the solid state of **5** are, as happened with compound **1**, oriented parallel to length of the crystals (Figure S23).

Synthesis and Structure of DTBA based compounds. We further explored the assembly of the ditopic ligand 1,4-dithiobenzamide (DTBA) with CuI. Thus, the equimolar reaction between CuI and DTBA in MeCN:DMF (20:1) solvent mixture at room temperature, led to 2D coordination polymer $\{[\text{CuI}(\text{DTBA})]\cdot\text{DMF}\}_n$, **6**·DMF. The synthesis of CuI-DTBA based compounds is gathered in Scheme 2. When **6**·DMF was soaked in acetonitrile or methanol, the exchange of guest solvent molecules took place and **6**·S, (S= MeCN, MeOH) were obtained. The exchange of the solvent molecules was confirmed by FT-IR analysis (Figure S37). Besides, **6**·S compounds displayed similar XRPD patterns, (Figure S38), confirming similar structures.

Otherwise, the reaction between CuI and DTBA (1:1) in refluxing acetonitrile, allowed to obtain single crystals of $\{[\text{CuI}(\text{DTBA})]\cdot 2\text{MeCN}\}_n$, **6**·2MeCN. However, crystals of **6**·2MeCN easily undergo a partial solvent loss under ambient conditions, giving rise to **6**·MeCN (Figure S39). Furthermore, **6**·2MeCN crystals could be also obtained from hot acetonitrile solutions of **6**·S (S= DMF, MeCN, MeOH).



Scheme 2. Synthetic routes of CuI-DTBA coordination compounds formation.

Compounds $\mathbf{6}\cdot\text{DMF}$ and $\mathbf{6}\cdot 2\text{MeCN}$ both display a 2D polymeric structure where the layers are parallel to the *bc* plane, with the solvent molecules lodged in the square interstitial spaces (Figure 4). In both cases the asymmetric unit entails a copper(I) atom, an iodine and two halves of the DTBA ligand, plus one DMF solvent molecule ($\mathbf{6}\cdot\text{DMF}$) or two acetonitrile ones ($\mathbf{6}\cdot 2\text{MeCN}$) as depicted in Figures S12 and S14. The copper atom displays a CuI_2S_2 coordination environment while the DTBA ligands are coordinated to one metal atom by each of the two opposite S atoms, and the iodine atom is bridging two Cu(I) atoms yielding Cu_2I_2 rhombi.

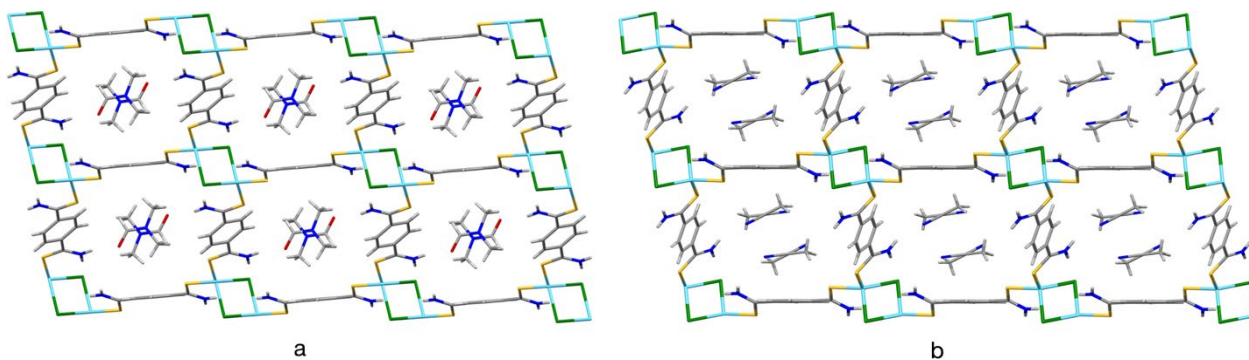


Figure 4. View of the 2D coordination polymers parallel to the (011) plane in **6**·DMF (a) and **6**·2MeCN (b) (Cu: cyan, I: green, S: yellow, N: dark blue, O: red, C: gray, H: white).

The solvent molecules are joined to the 2D polymeric layers by N-H···O bonds in **6**·DMF (Figure S18). In the structure of **6**·2MeCN it is interesting to note that the two solvent molecules are not equally bonded to the 2D framework: one of the MeCN molecules is joined to the CP layer by a N-H···N bond (Figure S19), while the second one is only weakly bonded to the former one by a C-H···N interaction (Table S67). This fact could explain the easy loss of one of the solvent molecules in **6**·2MeCN to yield **6**·MeCN. It was also observed that **6**·2MeCN was not stable in normal conditions, and for this compound only diffraction data at low temperature could be collected to solve the crystal structure.

Thermal Stability. Thermogravimetric analyses (TGA) of all synthesized CuX-TBA (X= I, Br) 1D CPs **1**, **1**·S (S= THF, acetone, MeOH), **4**, **5** and **5**·S (S= THF, acetone) were carried out under nitrogen atmosphere (Figures S40-47 and Table S68). For solvated compounds (**1**·S and **5**·S), upon heating, an initial solvent loss process was observed, with well-defined plateaus above *ca.* 100 °C. At higher temperatures, all compounds show a weight loss step between 250 and 275 °C, which could be assigned to the loss of TBA ligand.

The thermal stability of **6**·S (S= DMF, MeCN, MeOH) was also evaluated. Results shown an analogous thermal behavior for all the compounds (Figures S48-50 and Table S69). Thus, TGA curves displayed an initial weight loss which corresponds to the loss of one solvent molecule. Then, decomposition of the frameworks occurs in two consecutive steps, which correspond to the loss of half of the DTBA molecules. Additionally, the thermal stability of **6**·DMF was examined by XRPD after heating the samples at different temperatures for 1 h (Figure S51).

Hence, when **6**·DMF was heated above *ca.* 100 °C, a new phase was found. FT-IR and elemental analysis characterization of the solid heated at 225 °C (Figure S52 and Table S70) revealed a chemical composition of Cu₂I₂(DTBA), which corresponds to the loss of one half of DTBA ligand observed in TGA.

Vapor-Assisted Structural Transformations. The obtention of solvated and desolvated 1D networks prompted us to study the solvation/desolvation processes displayed by these compounds. To this end, experiments were followed up (*ex situ*) by XRPD to assess any phase changes. Initially, **1** and **5** were exposed to THF, acetone and MeOH vapors for 24 h at room temperature, in attempts to facilitate the inclusion of solvent guest molecules. Interestingly, after **1** exposure to THF and acetone vapors, the corresponding solvated CPs **1**·THF and **1**·acetone were formed, respectively (Figures 5a, b). The resulting solids were placed under vacuum for 24 h at room temperature, but no changes were detected. Then, solvated **1**·THF and **1**·acetone were heated at 80 °C under vacuum for 12 h, showing that solvent loss (**1**·S→**1**) was accompanied by concomitant formation of **4**. In the case of **5**, after exposure to THF and acetone vapors, both solvated and desolvated species (**5** + **5**·S) were identified (Figures 5c,d) indicating that transformation was not fully achieved. This can be attributed to the required rearrangement of the Cu₂IS rhombi in **5** to form alternated Cu₂I₂ and Cu₂S₂ rhombi to give rise to solvated species **5**·S. Then, the solvent removal was performed under the same conditions (80 °C in vac, 24 h) yielding desolvated compound **5**. Otherwise, no phase changes were detected after **1** and **5** exposure to MeOH vapor.

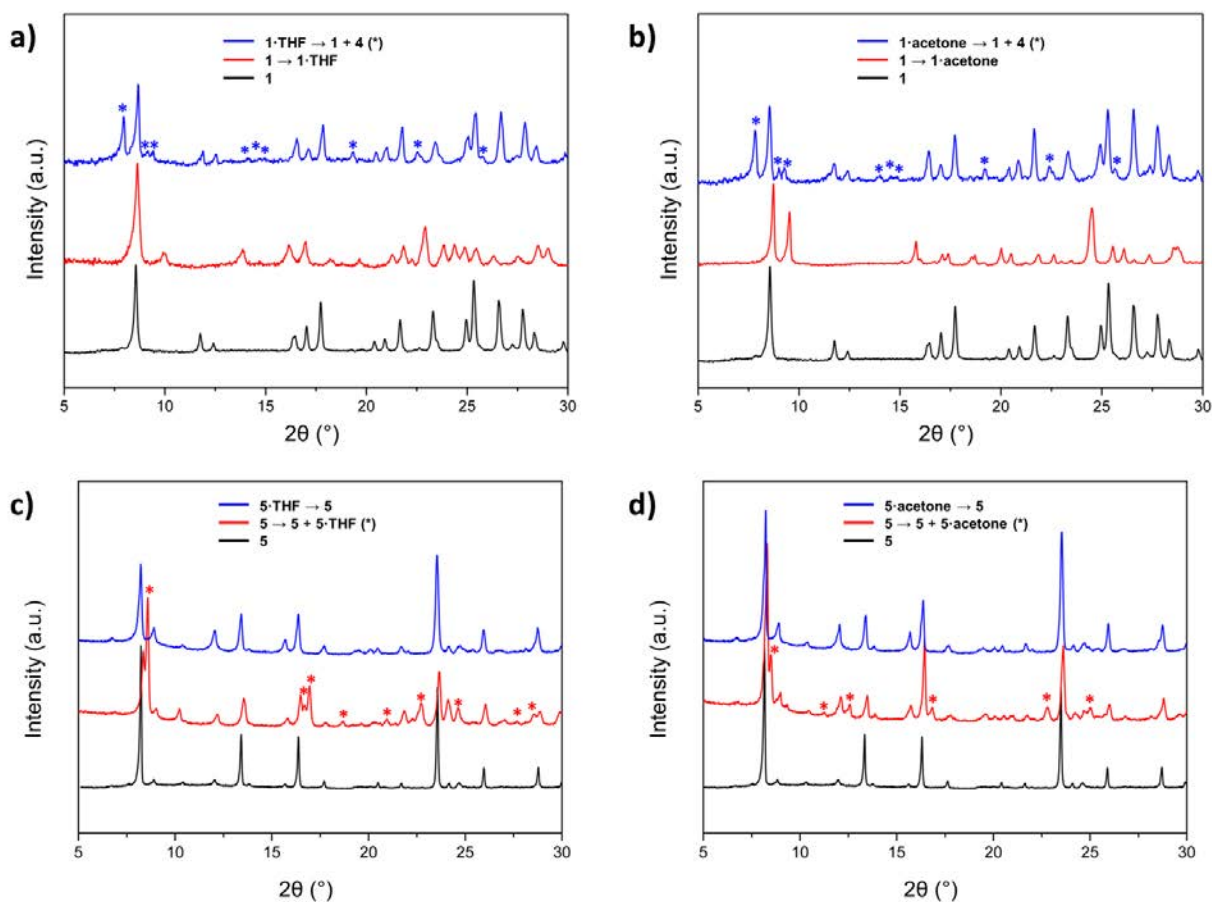


Figure 5. XRPD patterns of **1** (a,b) and **5** (c,d) before (black) and after exposing to THF or acetone vapors for 24 h at room temperature (red) and subsequent heating at 80 °C under vacuum for 12 h (blue). The asterisks indicate the peaks corresponding to **4** (a,b), **5·THF** (c) and **5·acetone** (d) phases.

Luminescent properties. Much research interest has recently focused on the luminescent properties of coordination polymers due to their potential applications as light emitting diodes.¹⁸ Indeed, some Cu(I) complexes have shown rich structural variety combined to brightly luminescent, even at room temperature, and emissive behavior that can be modulated with structure and environment.¹⁹ This facts prompted us to investigate the luminescent properties of

the synthesized compounds in the solid state upon excitation with a UV lamp ($\lambda_{\text{exc}} = 365 \text{ nm}$). At room temperature **1**, **1**·acetone and **1**·MeOH showed by naked eye, orange emission while no emission was observed for the other compounds. Moreover, when crystalline samples of **1**, **1**·S (S= THF, acetone, MeOH), **5** and **5**·S (S= THF, acetone), were immersed in liquid nitrogen and exposed to the irradiation of the same UV lamp, a clearly orange emission were observed. These changes were distinguished by naked eye and recorded by a digital camera (Figure 6). These processes are fully-reversible for all compounds returning to their initial state after they were allowed to stay at room temperature for few seconds. However, when compounds **2**, **3**, **4**, and **6**·S (S= DMF, MeCN, MeOH) were immersed in liquid nitrogen and then exposed to the UV irradiation, using the same UV lamp, any change was observed (Figure S53).

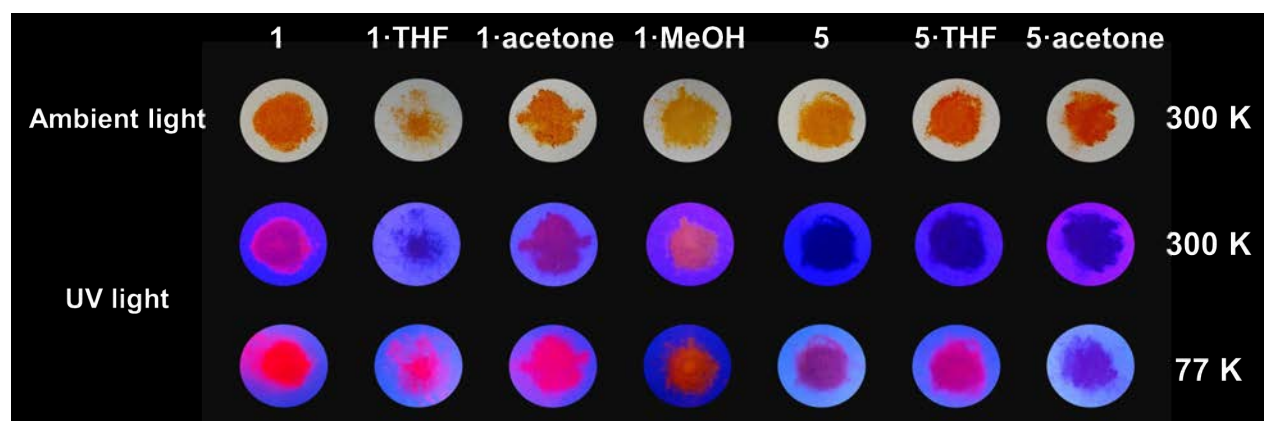


Figure 6. Photos of solid samples of 1D CPs **1**, **1**·S (S= THF, acetone, MeOH), **5** and **5**·S (S= THF, acetone) under ambient light and under UV lamp irradiation at 356 nm at room temperature (300 K) and in liquid nitrogen (77 K).

In order to check the possible presence of emission arising from the ligand, free TBA ligand was investigated. Solid state emission spectra at room temperature ($\lambda_{\text{exc}} = 359 \text{ nm}$) showed very weak emission in high energy region with maxima centered at *ca.* 424, 471, 483 and 493 nm, being

assigned to ligand-centered $\pi \rightarrow \pi^*$ transitions. (Figure S54). These bands appear as very weak in the blue region for **1**, **1**·S, **5** and **5**·S CPs.

To get more insight into the nature of the modest but fully reversible thermochromic effects found for all **1**, **1**·S (S= THF, acetone, MeOH), **5** and **5**·S (S= THF, acetone) compounds, the emission spectra were registered at variable temperature (from 300 to 100 K, $\lambda_{exc}= 450$ nm). For **1** and **1**·S (S= THF, acetone, MeOH), at room temperature weak broad bands with maximum centered a *ca.* 635, 630, 630 and 611nm respectively are observed. By lowering the temperature, broad and unstructured bands begin to appear, increasing their intensity as the temperature is decreasing. For **1** and **1**·MeOH, this broad band is progressively resolved as the temperature is decreasing showing a maximum centered at *ca.* 630 and 607 nm respectively at 80 K. **1**·THF and **1**·acetone have a similar behavior, a broad band centered at 630 nm is observed at 240 K and as the temperature is decreasing, it is going narrowing down having at 100 K, a band centered at 615 and 626 nm, respectively, together with a shoulder to lower energy (670 nm for **1**·THF) and another band at 657 nm for **1**·acetone (Figure 7). The emission lifetimes at 100 K are in the range 11 μ s (**1**)-16 μ s (**1**·S) and this microsecond time scale is indicative of an emission arising from a triplet state.

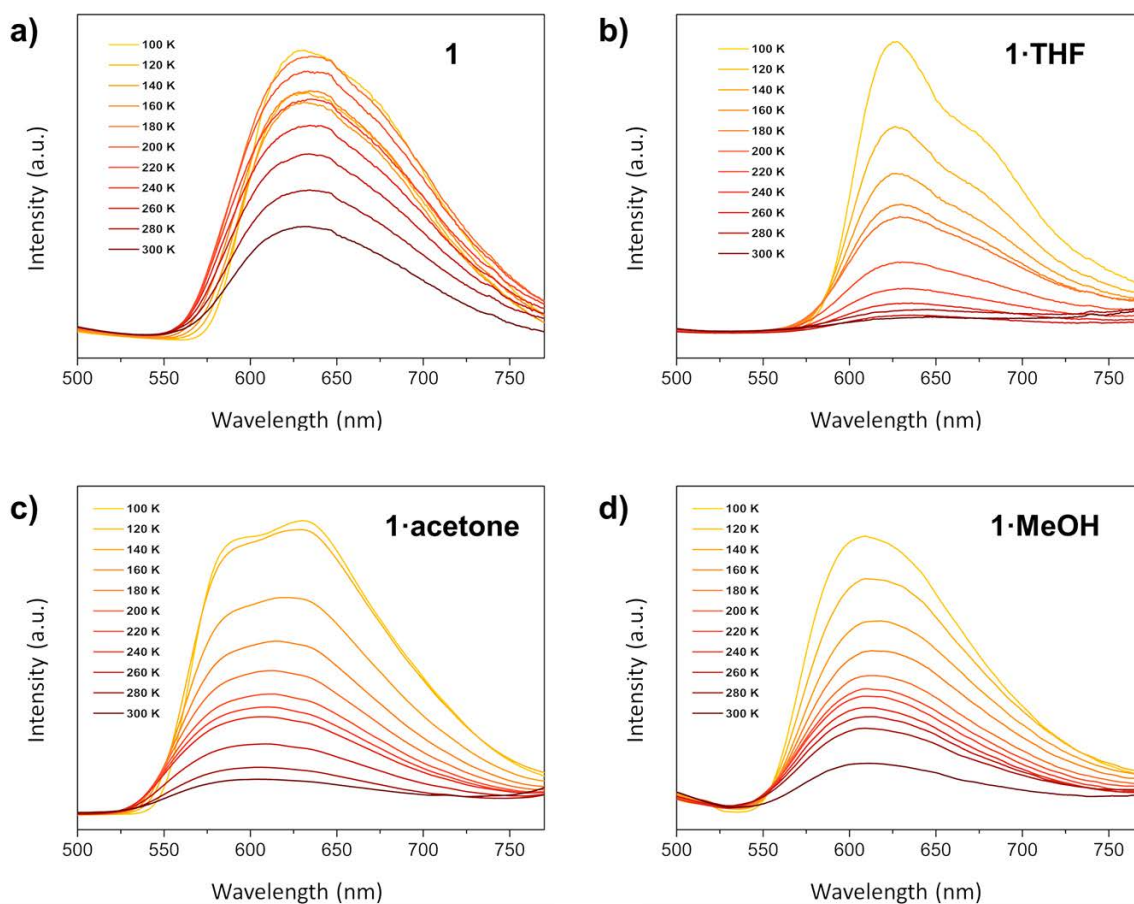


Figure 7. Temperature-dependent luminescence spectra of **1**·S (S= THF, acetone, MeOH) from 300 K down to 100 K in the solid state ($\lambda_{\text{exc}} = 450 \text{ nm}$; $\Delta T = 20 \text{ K}$).

The isostructural CPs based on copper bromide, **5** and **5**·S (S= THF, acetone) show lower emission than the analogous copper iodide **1** and **1**·S. From room temperature up to 180 K are not luminescent. However, when the temperature decreases weak broad emission bands begin to appear and at 80 K, broad bands centered at *ca.* 620, 682 and 638 nm respectively are observed (Figure 8). The emission lifetimes at 100 K are close to 10 μs being also indicative of an emission arising from a triplet state.

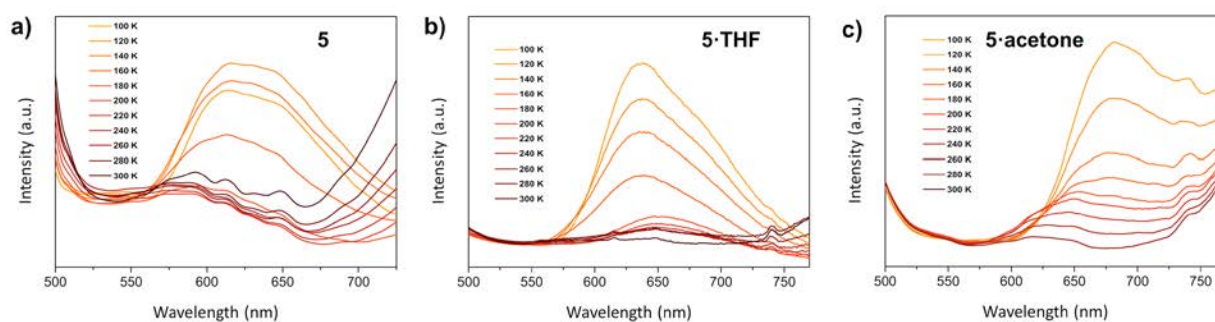


Figure 8. Temperature-dependent luminescence spectra of **5** and **5·S** (S= THF, acetone) from 300 K down to 100 K in the solid state ($\lambda_{exc}= 450$ nm; $\Delta T= 20$ K).

According to previous studies related to CPs based on copper halide, the origin of the observed emission centered around 610-680 nm might be derived from an excited state 3XLCT in character, which is itself a combination of halide to ligand charge transfer (3XLCT) and metal-centered transfer ($^3MCC: 3d^{10} \rightarrow 3d^9 4s^1 Cu$), being this 3MCC contribution very sensible to Cu \cdots Cu distances.^{3a, 20} The nature of the emission spectra, with broad and unstructured bands, are also in agreement with the assignation made as a combination of $^3(M+X)LCT$ states.²¹

In order to know deeply the nature of the origin of the observed thermochromism, the crystal structures for **1**, **1·S** (S= THF, acetone, MeOH), **5** and **5·S** (S= THF, acetone) were determined by single-crystal X-ray diffraction analysis at 110 K. As shown in Table 1, in all compounds a slight decreasing of cell parameters is observed; together with that, at lower temperature, for isostructural **1**, **1·S** (S= THF, acetone, MeOH) **5** and **5·S** (S= THF, acetone,) compounds, shortening in Cu \cdots Cu interactions are observed ($\Delta= 0.09$ and 0.056 nm for **1**, $\Delta= 0.07$ and 0.045 nm for **1·acetone**, $\Delta= 0.023$ and 0.060 nm for **1·THF**, $\Delta= 0.022$ and 0.047 nm for **1·MeOH**) for Cu₂I₂ and Cu₂S₂ rhomboids respectively and $\Delta= 0.025$ and 0.025 nm for **5**, $\Delta= 0.009$ and 0.00 nm for **5·acetone** and $\Delta= 0.023$ and 0.060 nm for **5·THF**) for Cu₂Br₂ and Cu₂S₂ rhomboids respectively. These

shortenings in the unit cell parameter and in the Cu···Cu distances at lower temperature are in accordance with the assignment made as a combination of $^3(M + X)LCT$ states,²¹ where the contribution of 3MCC transition to the emission is stronger when shorter are the Cu···Cu distances. Comparing the (Cu···Cu) distances for Cu₂X₂ rhomboids, we can observe that compounds containing Cu₂I₂ units (**1** and **1**·S) show shorter values (between 2.680 – 2.941 Å) than the analogous with Cu₂Br₂ units (**5** and **5**·S) (2.857-3.001Å). These facts are in agreement with the higher emission observed for compounds based on copper iodide (**1** and **1**·S) respect to those containing copper bromide (**5** and **5**·S) and support the 3MCC contribution in the emission. This is also supported by DFT calculations carried out, where the valence band is mostly formed by electronic states from the metallic chain, whilst the conduction band, and its closest empty states, are formed by electronic states located on the organic ligands, thus allowing the tunability of the compounds. In addition, the increase observed in the emission intensity upon cooling is due to an increase in structural rigidity, decreasing the non-radiative rate constant.

The photoluminescent spectra for **1**·S (S= acetone, THF, MeOH) are slightly dependent on the solvent molecules, being **1**·THF that shows higher emission. This observation could be attributed to a stronger hydrogen bond, with N-H····O distances (1,98Å) shorter than in **1**·acetone (2.04 Å) and **1**·MeOH (2.06 Å).

Table 1. Selected bond lengths for compounds **1**, **1**·S (S = THF, acetone, MeOH), **5** and **5**·S (S= THF, acetone) at different temperatures.

		Cu-Cu (Å)	Cu-X (Å)	Cu-S (Å)
1	296 K	2.689(2)	2.612(1)	2.277(2)
		2.967(2)	2.650(1)	2.511(2)
	110 K	2.940(3)	2.622(2)	2.295(2)
		3.003(3)	2.629(2)	2.534(3)

1 ·THF	296 K	2.940(3) 3.003(3)	2.622(2) 2.629(2)	2.295(2) 2.534(3)
	110 K	2.917(2) 2.969(2)	2.627(1) 2.638(1)	2.295(1) 2.480(1)
1 ·acetone	296 K	2.869(2) 2.876(1)	2.6137(8) 2.6356(8)	2.292(2) 2.529(2)
	110 K	2.815(1) 2.870(1)	2.6149(7) 2.6319(7)	2.295(1) 2.480(1)
1 ·MeOH	296 K	2.7128(9) 2.743(1)	2.6118(5) 2.6583(5)	2.294(1) 2.503(1)
	110 K	2.6914(6) 2.6963(6)	2.6158(3) 2.6526(3)	2.2963(7) 2.4726(7)
5	250 K		2.498(3) 2.600 (3) 2.600 (3)	2.280 (5) 2.341 (5) 2.342 (5)
			2.857 (3) 2.885 (3) 2.885 (3)	2.581(3) 2.494(3)
				2.271 (5)
5	110 K		2.498(3) 2.595(3) 2.595(3)	2.274(5) 2.341(5) 2.336(5)
			2.832(4) 2.860(4) 2.860(4)	2.575(3) 2.496(3)
				2.265(5)
5 ·THF	296 K	2.824 (1) 3.001 (1)	2.4674 (8) 2.4931 (8)	2.498 (2) 2.274 (1)
	110 K	2.7640 (9) 2.9781 (9)	2.4749 (6) 2.4738 (6)	2.445 (1) 2.271 (1)
5 ·acetone	200 K	2.813 (3) 2.989 (2)	2.475 (2)	2.270 (3) 2.471 (3)

Finally, the $^3(M + X)LCT$ band for **1-4** compounds is assigned based on the fact that related CPs containing thioacetamide ligands $[CuX(TAA)]_n$ ($X = Br, I$) instead thiobenzamide ligands are non-emissive in this region.^{9a} This feature could be attributed to the lack of π^* orbitals necessary for the halide to ligand charge transfer process.

Therefore, we can conclude that for **1-4** compounds, the emission bands, observed at room temperature, are due to a combination of 3XLCT and 3MCC states, while at lower temperatures a higher contribution of the metal-centered transfer (3MCC ; $d^{10}Cu \rightarrow d^9s^1Cu$) bands take place. These studies show direct evidences suggesting thermochromic luminescence of these compounds is caused by temperature-dependent which affect to $Cu \cdots Cu$ distances, being these $Cu \cdots Cu$ interactions the key parameter determining the 3CC transitions affecting their luminescence.

Electrical Conductivity. The electrical conductivity of the obtained CPs was evaluated in the solid state at 25 °C by using the two-contact method with a graphite paste contact (Figure S55). The conductivity values obtained under these conditions are summarized in Table 2.

Table 2. Electrical conductivity values obtained for the different coordination polymers at 25 °C using two contact method and average Cu-Cu, Cu-X and Cu-S distances.

	Conductivity (S/cm)	CB-VB gap (eV)
1 ^a	3.3 10 ⁻¹¹	1.38
1 ·acetone ^b	1.3 10 ⁻⁸	1.22
1 ·MeOH ^b	1.15 10 ⁻⁹	1.36
4 ^b	1.7 10 ⁻¹⁰	1.29
5 ^a	3.6 10 ⁻⁸	1.23
5 ·THF ^b	1.9 10 ⁻⁷	1.21
5 ·acetone ^b	1.5 10 ⁻⁹	1.27

^a Pellet. ^b Crystal.

The data obtained show that these CPs have a relatively low conductivity, within the range of semiconductor materials, with no significant differences between them. The electrical conductivity of a close related one-dimensional CPs based on Cu₂I₂S₂ chains, similar to that showed in compound **1**, has recently been reported showing a semiconductor behavior and conductivity value of 6.8 10⁻⁹ S/cm at 25 °C.²² This is quite in agreement with the values obtained for compounds **1** and **1**·S (S= THF, acetone, MeOH). Others related 2D and 3D CPs with both sulfur and iodine atoms acting as bridging ligands and similar Cu-S-Cu-I chains, show conductivity values in the range 10⁻⁷-10⁻⁹ S/cm which are in the range of those values observed for **1**, **1**·S, **4** and **5**.^{9a, 23}

A structural analysis can help to rationalize these conductivity values. Thus, the short Cu-Cu, Cu-I and Cu-S distances (Table 1) and the chain angles (Tables S40-62) are probably the key to understand the electrical conductivity in these 1D-2D CPs since they affect to the electron delocalization taking place along the chains as a consequence of the copper (d_z), halogen and sulfur (p_z) orbital overlapping, *i.e.* a more effective overlap between these orbitals, give raise better electrical conductivity which typically imposes a shortening in the distances. As expected, the obtained values for **1**, **1**·THF and **5** are *ca.* one-two orders of magnitude smaller than those obtained using micrometer crystals. This difference is due to the well-known effect of the inter-grain contacts that increases the resistivity in the pellets.

Computed Density of Electronic States. For a deeper rationalization of the physical properties, theoretical calculations on these CPs were carried out. Figure 9 shows the computed density of electronic states (in arb. units) for the different compounds of the present study as a function of the energy referred to the Fermi level (in eV). Besides the total density of states, we have also computed the projected density of states (PDOS) onto the organic ligands, onto the metallic chains, as well as onto the functional groups THF, Acetone and MeOH. For all the cases theory predicts a canonical narrow-gap semiconducting character with electronic gaps ranging between 1.2—1.5 eV, where most of the compounds behave as n-type semiconductors (with the Fermi level almost pinning the conduction band, CB), excepting **5** and **5**·acetone systems, which exhibit a p-type semiconducting character with the Fermi level pinning the valence band, VB.

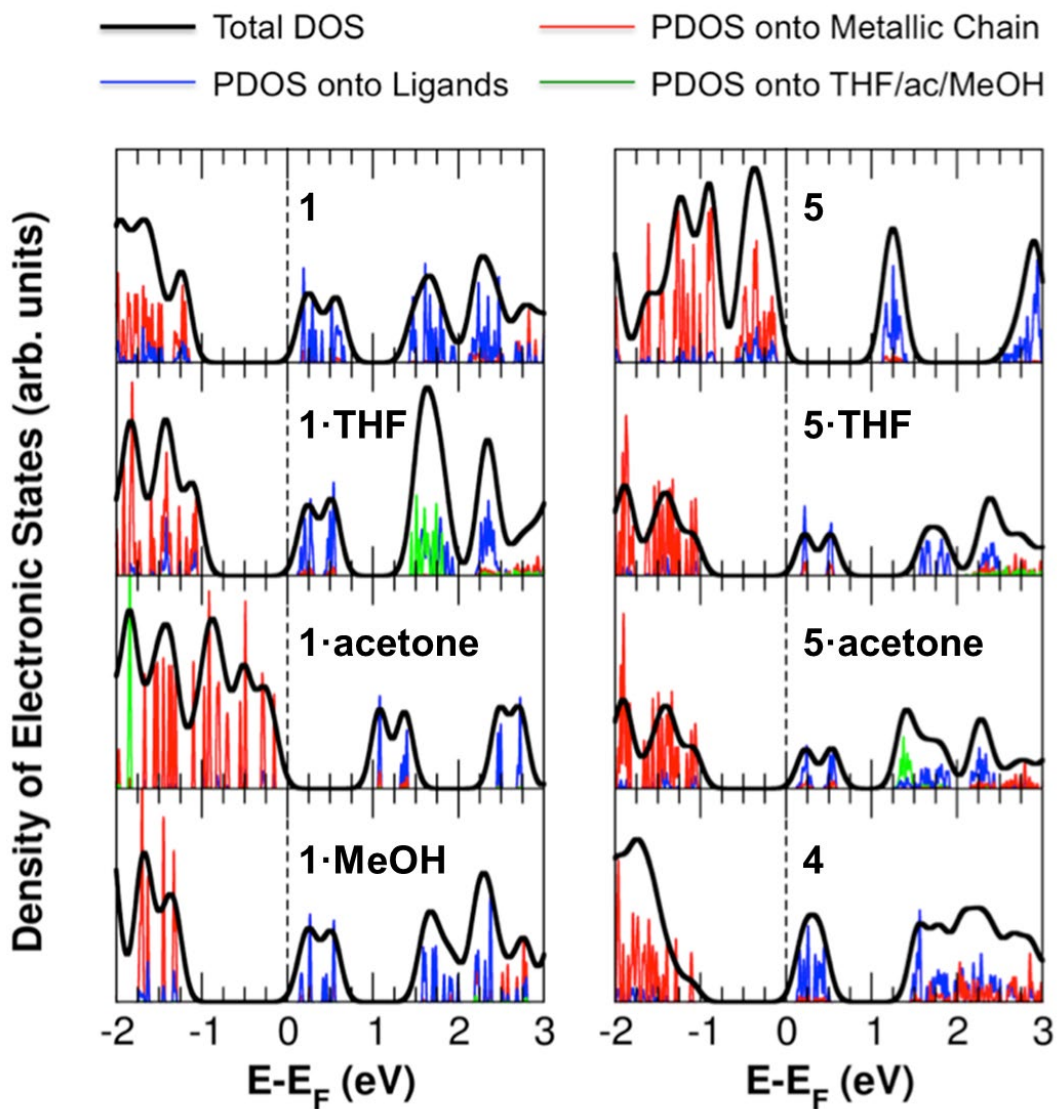


Figure 9. Computed total density of electronic states (in arb. units) for the different compounds, as a function of the energy referred to the Fermi level (in eV), is depicted by a black line. Projected density of states (PDOS) onto the organic ligands, onto the metallic chains, and onto the THF, acetone and MeOH molecules are depicted by blue, red and green lines, respectively.

It is interesting to notice that a fair correlation can be found between the computed band-gap values with the experimental conductivity ones (Table 2). As the conductivity values increase across the different compounds the computed CB-VB gaps decrease. Additionally, although all

the band-gap values lie in a very narrow window, a noticeable change is theoretically predicted between the **1**·acetone (1.22 eV) and the **1**·MeOH (1.36 eV) compounds, the latter being close to the case of compound **1**. On the other hand, it is also interesting how the band-gap values computed for **5**, **5**·THF and **5**·acetone compounds are very close ranging between 1.21 and 1.27 eV.

Additionally, due to the high structural symmetry of the compounds, the electronic degeneracy of the electronic states, close to the Fermi level, show electronic multiplicity. Density of states profiles show remarkable similarities for all the compounds. It is interesting to notice how the conduction band, and a set of close electronic states, yields in all cases one or two-peak features. These electronic states will be of particular importance in the analysis of the optical properties; being the electronic states, together with the valence band, involved in the most important optical transitions within the experimental range of interest (450—750 nm).

Regarding the PDOS profiles for all cases it is possible to observe, as expected in this kind of compounds, that the valence band is mostly formed by electronic states from the metallic chain, whilst the conduction band, and its closest empty states, are formed by electronic states located on the organic ligands. For those compounds incorporating THF, acetone and MeOH from the synthesis, the electronic states associated to these functional groups locate far from the gap region, which will not have influence in the optical properties beyond their structural influence in the crystal-cell relaxation. It is important to remark how, depending on each specific compound, induced electronic states of the metallic chain reflect in the conduction band region, or induced electronic states of the organic ligands reflect in the valence band. This observation is related with the overlapping degree between valence and conduction states, which will have its reflection in the efficiency of the optical transitions between such states.

Excitation Spectra: TDDFT + CIS. Figure S56 shows the computed TDDFT photoexcitation spectra for the different compounds as a function of the photon wavelength (in nm) for structures resolved at two different temperatures for each compound at standard pressure. As a first observation, one realizes that all the spectra, within the wavelength region of experimental interest (450—750 nm), show a two-peak feature, excepting **4** that only exhibits a wide unique peak. The CIS method permits to compute the contribution (in %) of an electronic transition between two electronic states to a given excitation energy. In Figure S56 we show the most important electronic transitions contributing to each excitation peak. Specifically, in this study, the CIS-based analysis permits to assign to all the two-peak features two distinct and prominent transitions ($> 75\%$ of contribution): a low-energy excitation corresponding to electronic transitions between the VB and the CB (ranging between 620—635 nm at 110 K and 630—650 nm at RT), and the high-energy excitation corresponding to electronic transitions between the VB to the CB+1 (ranging between 560—580 nm at 110 K and 565—595 nm at RT). As mentioned, for the case of **4** just one wide peak is observed in this wavelength window, due to the high electronic degeneracy of its conduction band comprising a large number of electronic states with very similar eigen-energies. For this system, the 110 K and RT peaks are located at 604 and 622 nm (corresponding to VB→CB transition), respectively. Residual electronic transition contributions ($<25\%$) to the main excitations correspond to transitions between electronic states close but deeper than the VB and the CB and CB+1.

Interestingly, the photoexcitation intensity is more pronounced in all cases for the low-temperature structures. At this point it is important to remark that the differences observed between the different compounds within our theoretical formalism are exclusively due to the structural differences; no environmental temperature effects, such as temperature-induced band broadening,

can be captured by our approach beyond the reflection of temperature in the crystal structure. Nonetheless, the trend observed is consistent with the photoluminescence spectra and the associated photoelectronic decay. Besides, a slight shift towards lower photon energies is observed in all the structures. This behavior may be explained in terms of the electronic states narrowing in the high-temperature structures in the electronic states close to the gap. Most intense average photoexcitation signal is obtained for the compounds involving iodine, including **4**. It is also worth noticing that the gap between the high and low-energy excitations is slightly higher for these I-based compounds, for which the excitation intensity differences between the low and high-temperature structures are also more pronounced. On the other hand, regarding Figure S56, theory predicts a lower TDDFT photoexcitation response for the compounds involving bromine. This difference between the optical intensity in I and Br-based compounds may have its origin in the slight overlapping between the valence and conduction bands. In Figure S56, for Br-based compounds, it is possible to appreciate how some induced reflection of the metallic chain electronic states appear in the conduction band and *vice-versa*. This slight overlapping between states with different electronic character (metallic/organic) could decrease the efficiency of the electronic transitions, reducing the photoexcitation intensity. This effect is also observable in the experiments.

As explained in previous section, computed PDOS profiles of Figure S56 shows the VB mostly located at the metallic chains, whilst the CB and CB+1 are spatially located fundamentally in the organic ligands. Thus, the electronic origin of the transitions reported here is purely metallorganic (i.e. metal-ligand transitions). 3D morphology and spatial distribution and location of the VB, CB and CB+1 for all the compounds analyzed here can be found depicted in Figure S57. In this figure,

the 3D orbital isodensities corresponding to the VB, CB and CB+1 states are represented all for an isodensity value of 10^{-4} a.u.

To conclude, it is worth mentioning that, from the theoretical analysis, the THF, acetone and MeOH molecules present in some of the crystals do not seem to have any influence in the optical properties, which do not contribute electronically to the VB, CB or CB+1 states (Figure S56), responsible of the most pronounced optical transitions. This evidence is also visible in Figure S57.

Conclusions

In summary, this work shows the high structural versatility of the structurally simple thiobenzamide ligands. In particular, it presents results of the direct reactions, under ambient conditions, of thiobenzamide (TBA) and dithiobenzamide (DTBA) with CuX (X= I, Br). These reactions gave rise to multifunctional 1D- and 2D-CPs. The isolated 1D-CPs [CuI(TBA)]_n (**1**) and [CuBr(TBA)·S]_n (**5**) showed the ability to accommodate a variety of organic solvents located in their structures, leading to the solvated species [CuI(TBA)·S]_n (**1·S**) (S= THF, acetone, methanol) and [CuBr(TBA)·S]_n (**5·S**) (S= THF, acetone). Interestingly the electronic properties, *i.e.* luminescence and electrical semiconductivity, of **1·S** or **5·S** are significantly different allowing VOCs detection. Thus, for instance, **1** is able to detect the presence of THF or acetone at room temperature, while **5** only at low temperature. Theoretical calculations have been used to rationalize these findings.

This work paves new possibilities in terms of structural and material chemistry for the use of thioamide ligands.

ASSOCIATED CONTENT

Supporting Information. A pdf file with additional experimental information, theoretical studies and physical properties is available free of charge. Files in CIF format for compounds **1-3** are (CCDC refs.: 1835539-1835559) available free of charge.

Acknowledgments. MINECO (MAT2016-77608-C3-1-P, MAT2016-75883-C2-1-P, MAT2017-85089-C2-1-R; Ramon y Cajal: RYC-2015-17730), Ministerio de Ciencia, Innovación y Universidades (CTQ2016-75816-C2-1-P) and European Union's Horizon 2020 research and innovation programme (Grant 785219; Graphene Flagship –core2).

REFERENCES

1. S. R. Batten, S. M. N., D. R. Turner, *Coordination Polymers: Design, Analysis and Application*. 2009.
2. (a) Hassanein, K.; Conesa-Egea, J.; Delgado, S.; Castillo, O.; Benmansour, S.; Martínez, J.-I.; Abellán, G.; Gómez-García, C.-J. C.; Zamora, F.; Amo-Ochoa, P, Electrical Conductivity and Strong Luminescence in Copper Iodide Double Chains with Isonicotinato Derivatives. *Chem. Eur. J.* **2015**, *21*, 17282-17292; (b) Amo-Ochoa, P.; Hassanein, K.; Gomez-Garcia, C. J.; Benmansour, S.; Perles, J.; Castillo, O.; Martinez, J. I.; Ocon, P.; Zamora, F., Reversible Stimulus-Responsive Cu(I) Iodide Pyridine Coordination Polymer. *Chem. Commun.* **2015**, *51*, 14306-14309; (c) Delgado, S.; Sanz Miguel, P. J.; Priego, J. L.; Jiménez-Aparicio, R.; Gómez-García, C. J.; Zamora, F., A Conducting Coordination Polymer Based on Assembled Cu₉ Cages. *Inorg. Chem.* **2008**, *47*, 9128-9130; (d) Gallego, A.; Castillo, O.; Gómez-García, C. J.; Zamora, F.; Delgado, S., Electrical Conductivity and Luminescence in Coordination Polymers Based on Copper(I)-Halides and Sulfur-Pyrimidine Ligands. *Inorg. Chem.* **2012**, *51*, 718-727.

3. (a) Ford, P. C.; Cariati, E.; Bourassa, J., Photoluminescence Properties of Multinuclear Copper(I) Compounds. *Chem. Rev.* **1999**, *99*, 3625-3648; (b) Wing-Wah Yam, V.; Kam-Wing Lo, K., Luminescent Polynuclear D10 Metal Complexes. *Chem. Soc. Rev.* **1999**, *28* (5), 323-334.
4. (a) Blake, A. J.; Champness, N. R.; Hubberstey, P.; Li, W.-S.; Withersby, M. A.; Schröder, M., Inorganic Crystal Engineering Using Self-Assembly of Tailored Building-Blocks. *Coord. Chem. Rev.* **1999**, *183*, 117-138; (b) Peng, R.; Li, M.; Li, D., Copper(I) Halides: A Versatile Family in Coordination Chemistry and Crystal Engineering. *Coord. Chem. Rev.* **2010**, *254*, 1-18; (c) Graham, P. M.; Pike, R. D.; Sabat, M.; Bailey, R. D.; Pennington, W. T., Coordination Polymers of Copper(I) Halides. *Inorg. Chem.* **2000**, *39*, 5121-5132.
5. (a) Cariati, E.; Lucenti, E.; Botta, C.; Giovanella, U.; Marinotto, D.; Righetto, S., Cu(I) Hybrid Inorganic–Organic Materials with Intriguing Stimuli Responsive and Optoelectronic Properties. *Coord. Chem. Rev.* **2016**, *306*, 566-614; (b) Tsuge, K.; Chishina, Y.; Hashiguchi, H.; Sasaki, Y.; Kato, M.; Ishizaka, S.; Kitamura, N., Luminescent Copper(I) Complexes with Halogenido-Bridged Dimeric Core. *Coord. Chem. Rev.* **2016**, *306*, 636-651; (c) Li, J.-C.; Li, H.-X.; Li, H.-Y.; Gong, W.-J.; Lang, J.-P. Ligand Coordination Site-Directed Assembly of Copper(I) Iodide Complexes of ((Pyridyl)-1-pyrazolyl)pyridine. *Cryst. Growth Des.* **2016**, *16*, 1617-1625.
6. (a) Zhu, H.-B.; Gou, S.-H., In Situ Construction of Metal–Organic Sulfur-Containing Heterocycle Frameworks. *Coord. Chem. Rev.* **2011**, *255*, 318-338; (b) Yang, X.-J.; Li, H.-X.; Xu, Z.-L.; Li, H.-Y.; Ren, Z.-G.; Lang, J.-P. Spacer length-controlled assembly of [CunIn]-based coordination polymers from CuI and bis(4-phenylpyrimidine-2-thio)alkane ligands. *CrystEngComm* **2012**, *14*, 1641-1652; (c) Li, H.-X.; Zhao, W.; Li, H.-Y.; Xu, Z.-L.; Wang, W.-X.; Lang, J.-P. [Cu₃₀I₁₆(mtpmt)₁₂(μ₁₀-S₄)]: an unusual 30-membered copper(i) cluster derived

from the C–S bond cleavage and its use in heterogeneous catalysis. *Chem. Commun.* **2013**, *49*, 4259-426.

7. Lobana, T. S.; Sharma, R.; Bawa, G.; Khanna, S., Bonding and Structure Trends of Thiosemicarbazone Derivatives of Metals—an Overview. *Coord. Chem. Rev.* **2009**, *253*, 977-1055.

8. (a) Tristan, M.; Seda, C.; R., B. D. W.; M., F. M. M.; J., G. M. A.; M., D. W. B. F.; K., V. I.; W., M. E.; A., P. A. R., Thioamides: Versatile Bonds to Induce Directional and Cooperative Hydrogen Bonding in Supramolecular Polymers. *Chem. Eur. J.* **2013**, *19*, 8642-8649; (b) Eccles, K. S.; Morrison, R. E.; Maguire, A. R.; Lawrence, S. E., Crystal Landscape of Primary Aromatic Thioamides. *Cryst. Growth Des.* **2014**, *14*, 2753-2762; (c) Lytvynenko, A. S.; Kolotilov, S. V.; Cador, O.; Golhen, S.; Ouahab, L.; Pavlishchuk, V. V., Antiferromagnetic Ordering in Cobalt(Ii) and Nickel(Ii) 1d Coordination Polymers with the Dithioamide of 1,3-Benzenedicarboxylic Acid. *New J. Chem.* **2011**, *35*, 2179-2186.

9. (a) Troyano, J.; Perles, J.; Amo-Ochoa, P.; Martinez, J. I.; Zamora, F.; Delgado, S., Reversible Recrystallization Process of Copper and Silver Thioacetamide-Halide Coordination Polymers and Their Basic Building Blocks. *Crystengcomm* **2014**, *16*, 8224-8231; (b) Troyano, J.; Perles, J.; Amo-Ochoa, P.; Zamora, F.; Delgado, S., Strong Luminescent Copper(I) Halide Coordination Polymers and Dinuclear Complexes with Thioacetamide and N,N[Prime or Minute]-Donor Ligands. *CrystEngComm* **2016**, *18*, 1809-1817; (c) Javier, T.; Oscar, C.; I., M. J.; Vanesa, F.-M.; Yolanda, B.; Daniel, M.; Félix, Z.; Salome, D., Reversible Thermochromic Polymeric Thin Films Made of Ultrathin 2d Crystals of Coordination Polymers Based on Copper(I)-Thiophenolates. *Adv. Funct. Mater.* **2018**, *28*, 1704040.

10. Dixon, S.; Whitby, R. J., Efficient Synthesis of Thioamide Terminated Molecular Wires. *Tetrahedron Lett.* **2006**, *47*, 8147-8150.
11. (a) Gonze, X., Adiabatic Density-Functional Perturbation Theory. *Phys. Rev. A* **1995**, *52*, 1096-1114; (b) Baroni, S.; Giannozzi, P.; Testa, A., Green's-Function Approach to Linear Response in Solids. *Phys. Rev. Lett.* **1987**, *58*, 1861-1864; (c) Baroni, S.; de Gironcoli, S.; Dal Corso, A.; Giannozzi, P., Phonons and Related Crystal Properties from Density-Functional Perturbation Theory. *Rev. Mod. Phys.* **2001**, *73*, 515-562; (d) Rocca, D.; Gebauer, R.; Saad, Y.; Baroni, S., Turbo Charging Time-Dependent Density-Functional Theory with Lanczos Chains. *J. Chem. Phys.* **2008**, *128*, 154105; (e) Walker, B.; Gebauer, R., Ultrasoft Pseudopotentials in Time-Dependent Density-Functional Theory. *J. Chem. Phys.* **2007**, *127*, 164106; (f) Walker, B.; Saitta, A. M.; Gebauer, R.; Baroni, S., Efficient Approach to Time-Dependent Density-Functional Perturbation Theory for Optical Spectroscopy. *Phys. Rev. Lett.* **2006**, *96*, 113001.
12. Monkhorst, H. J.; Pack, J. D., Special Points for Brillouin-Zone Integrations. *Phys. Rev. B* **1976**, *13*, 5188-5192.
13. Perdew, J. P.; Burke, K.; Ernzerhof, M., Generalized Gradient Approximation Made Simple. *Phys. Rev. Lett.* **1996**, *77*, 3865-3868.
14. Vanderbilt, D., Soft Self-Consistent Pseudopotentials in a Generalized Eigenvalue Formalism. *Phys. Rev. B* **1990**, *41*, 7892-7895.
15. Frisch, M. J.; Trucks, G. W.; Schlegel, H. B.; Scuseria, G. E.; Robb, M. A.; Cheeseman, J. R.; Scalmani, G.; Barone, V.; Petersson, G. A.; Nakatsuji, H.; Li, X.; Caricato, M.; Marenich, A. V.; Bloino, J.; Janesko, B. G.; Gomperts, R.; Mennucci, B.; Hratchian, H. P.; Ortiz, J. V.; Izmaylov, A. F.; Sonnenberg, J. L.; Williams; Ding, F.; Lipparini, F.; Egidi, F.; Goings, J.; Peng, B.; Petrone, A.; Henderson, T.; Ranasinghe, D.; Zakrzewski, V. G.; Gao, J.; Rega, N.; Zheng, G.;

Liang, W.; Hada, M.; Ehara, M.; Toyota, K.; Fukuda, R.; Hasegawa, J.; Ishida, M.; Nakajima, T.; Honda, Y.; Kitao, O.; Nakai, H.; Vreven, T.; Throssell, K.; Montgomery Jr., J. A.; Peralta, J. E.; Ogliaro, F.; Bearpark, M. J.; Heyd, J. J.; Brothers, E. N.; Kudin, K. N.; Staroverov, V. N.; Keith, T. A.; Kobayashi, R.; Normand, J.; Raghavachari, K.; Rendell, A. P.; Burant, J. C.; Iyengar, S. S.; Tomasi, J.; Cossi, M.; Millam, J. M.; Klene, M.; Adamo, C.; Cammi, R.; Ochterski, J. W.; Martin, R. L.; Morokuma, K.; Farkas, O.; Foresman, J. B.; Fox, D. J. *Gaussian 16 Rev. B.01*, Wallingford, CT, 2016.

16. Foresman, J. B.; Head-Gordon, M.; Pople, J. A.; Frisch, M. J., Toward a Systematic Molecular Orbital Theory for Excited States. *J. Chem. Phys.* **1992**, *96*, 135-149.

17. A.T.H. Lenstra, S. T., W. Versichel, *Bull. Soc. Chim. Belg.* Crystal Structure of Cuprous Chloride Tri-thiobenzamide. **1977**, *86*, 419.

18. (a) Cariati, E.; Bu, X.; Ford, P. C., Solvent- and Vapor-Induced Isomerization between the Luminescent Solids [Cui(4-Pic)]₄ and [Cui(4-Pic)]_∞ (Pic = Methylpyridine). The Structural Basis for the Observed Luminescence Vapochromism. *Chem. Mater.* **2000**, *12*, 3385-3391; (b) Ciurtin, D. M.; Pschirer, N. G.; Smith, M. D.; Bunz, U. H. F.; zur Loye, H.-C., Two Luminescent Coordination Polymers with a Triple-Helix Structure: Hg₂(C₃H₂N₂)·CH₂Cl₂ (X = Cl and Br). *Chem. Mater.* **2001**, *13*, 2743-2745; (c) Wurthner, F.; Sautter, A., Highly Fluorescent and Electroactive Molecular Squares Containing Perylene Bisimide Ligands. *Chem. Commun.* **2000**, 445-446.

19. (a) Habib, H. A.; Hoffmann, A.; Höpfe, H. A.; Steinfeld, G.; Janiak, C., Crystal Structure Solid-State Cross Polarization Magic Angle Spinning 13c Nmr Correlation in Luminescent D10 Metal-Organic Frameworks Constructed with the 1,2-Bis(1,2,4-Triazol-4-Yl)Ethane Ligand. *Inorg. Chem.* **2009**, *48*, 2166-2180; (b) Yam, V. W.-W.; Wong, K. M.-C., Luminescent Metal

Complexes of D6, D8 and D10 Transition Metal Centres. *Chem. Commun.* **2011**, *47*, 11579-11592.

20. (a) Vega, A.; Saillard, J.-Y., Bonding in Tetrahedral Cu₄(M₃-X)₄ Copper(I) Clusters: A Dft Investigation. *Inorg. Chem.* **2004**, *43*, 4012-4018; (b) De Angelis, F.; Fantacci, S.; Sgamellotti, A.; Cariati, E.; Ugo, R.; Ford, P. C., Electronic Transitions Involved in the Absorption Spectrum and Dual Luminescence of Tetranuclear Cubane [Cu₄i₄(Pyridine)₄] Cluster: A Density Functional Theory/Time-Dependent Density Functional Theory Investigation. *Inorg. Chem.* **2006**, *45*, 10576-10584; (c) Perruchas, S.; Tard, C.; Le Goff, X. F.; Fargues, A.; Garcia, A.; Kahlal, S.; Saillard, J.-Y.; Gacoin, T.; Boilot, J.-P., Thermochromic Luminescence of Copper Iodide Clusters: The Case of Phosphine Ligands. *Inorg. Chem.* **2011**, *50* (21), 10682-10692; (d) Henline, K. M.; Wang, C.; Pike, R. D.; Ahern, J. C.; Sousa, B.; Patterson, H. H.; Kerr, A. T.; Cahill, C. L., Structure, Dynamics, and Photophysics in the Copper(I) Iodide–Tetrahydrothiophene System. *Cryst. Growth Des.* **2014**, *14*, 1449-1458; (e) Liu, Z.; Djurovich, P. I.; Whited, M. T.; Thompson, M. E., Cu₄i₄ Clusters Supported by PAN-Type Ligands: New Structures with Tunable Emission Colors. *Inorg. Chem.* **2012**, *51*, 230-236.
21. Zink, D. M.; Volz, D.; Baumann, T.; Mydlak, M.; Flügge, H.; Friedrichs, J.; Nieger, M.; Bräse, S., Heteroleptic, Dinuclear Copper(I) Complexes for Application in Organic Light-Emitting Diodes. *Chem. Mater.* **2013**, *25*, 4471-4486.
22. Givaja, G.; Amo-Ochoa, P.; Gomez-Garcia, C. J.; Zamora, F., Electrical Conductive Coordination Polymers. *Chem. Soc. Rev.* **2012**, *41*, 115-147.
23. Troyano, J.; Perles, J.; Amo-Ochoa, P.; Martínez, J. I.; Concepción Gimeno, M.; Fernández-Moreira, V.; Zamora, F.; Delgado, S., Luminescent Thermochromism of 2d

Coordination Polymers Based on Copper(I) Halides with 4-Hydroxythiophenol. *Chem. Eur. J.*
2016, 22, 18027-18035.

TOC. Novel Cu(I)-based 1D and 2D coordination polymers (CPs) has been synthesized by using mono- and ditopic thiobenzamide ligands, respectively. Since these CPs show the ability to accommodate solvent molecules in their structures, the luminescent and electrical properties of the different solvated compounds have been investigated and rationalized using theoretical calculations. Due to the different luminescent behavior depending on the solvent, 1D CPs show potential application for sensing volatile organic compounds (VOCs).

